



Nuclear deformation as a source of the nonlinearity of the King plot in the Yb⁺ ionSaleh O. Allehabi, V. A. Dzuba , and V. V. Flambaum *School of Physics, University of New South Wales, Sydney 2052, Australia*

A. V. Afanasjev

Department of Physics and Astronomy, Mississippi State University, Mississippi 39762, USA

(Received 7 December 2020; accepted 18 February 2021; published 3 March 2021)

We perform atomic relativistic many-body calculations of the field isotope shifts and calculations of corresponding nuclear parameters for all stable even-even isotopes of the Yb⁺ ion. We demonstrate that if we take nuclear parameters of the Yb isotopes from a range of the state of the art nuclear models, which all predict strong quadrupole nuclear deformation, and then calculate nonlinearity of the King plot caused by the difference in the deformation in different isotopes, the result is consistent with the nonlinearity observed in the experiment [I. Counts *et al.*, *Phys. Rev. Lett.* **125**, 123002 (2020)]. The changes of nuclear rms radius between isotopes extracted from experiment are consistent with those obtained in the nuclear calculations.

DOI: [10.1103/PhysRevA.103.L030801](https://doi.org/10.1103/PhysRevA.103.L030801)

In a recent paper [1], the nonlinearity of the King plot has been observed. The authors state that the effect may indicate physics beyond the standard model (SM), or that, within the SM, they may come from the quadratic field shift (QFS). Possible nonlinearity of the King plot in Yb⁺ was studied theoretically in Ref. [2]. In the present paper, we show that it is more likely that the observed nonlinearity of the King plot is due to a significant nonmonotonic variation of the nuclear deformation in the chain of isotopes. We perform nuclear and atomic calculations of the field isotope shift (FIS) which include nuclear deformation and demonstrate that the dependence of the deformation on isotopes leads to a nonlinearity of the King plot, which is consistent with the observations in Ref. [1]. We show that the comparison of theoretical and experimental nonlinearities can be used to discriminate between different nuclear models, favoring some and disfavoring others.

It is well known from experimental nuclear rotational spectra [3] and its theoretical interpretation [4,5] as well as from the nuclear calculations presented below that all even-even Yb isotopes studied in Ref. [1] have deformed nuclear ground states with the parameters of the quadrupole deformation $\beta \approx 0.3$. In our previous paper [6], we demonstrated that nuclear deformation may lead to a nonlinearity of the King plot.

Therefore, in the present paper we calculate FIS in even-even Yb isotopes with accounting for nuclear deformation. We treat Yb⁺ as a system with one external electron above closed shells and use the correlation potential method [7]. This approach works well for Yb⁺ as demonstrated in our earlier works [8–10]. We calculate the correlation potential $\hat{\Sigma}$ in the second order of the many-body perturbation theory. Correlation potential is the nonlocal (integration) operator responsible for the correlation corrections due to interaction between valence electron and electrons in the core. Then we use $\hat{\Sigma}$ to calculate the states of valence electron (numerated

by v) in the form of the Brueckner orbitals (BO):

$$(\hat{H}^{\text{HF}} + \hat{\Sigma} - \epsilon_v)\psi_v^{\text{BO}} = 0. \quad (1)$$

Here \hat{H}^{HF} is the relativistic Hartree-Fock (HF) Hamiltonian for the closed-shell core of Yb⁺,

$$\hat{H}^{\text{HF}} = c\hat{\alpha}_i \cdot \hat{p}_i + (\beta - 1)mc^2 + V_{\text{nuc}}(r_i) + V_{\text{core}}(r_i). \quad (2)$$

In this expression, α and β are the Dirac matrices, V_{nuc} is nuclear potential obtained by integrating nuclear charge density, V_{core} is the self-consistent HF potential, and the index i numerates single-electron states. This method is similar to the many-body perturbation theory (MBPT) method used in Ref. [1].

FIS is calculated by varying nuclear potential V_{nuc} in (2). The results are presented in the form of expansion over the change in nuclear momenta (see also Ref. [1]),

$$\nu_a^{\text{FIS}} = F_a \delta \langle r^2 \rangle + G_a^{(2)} \delta \langle r^2 \rangle^2 + G_a^{(4)} \delta \langle r^4 \rangle. \quad (3)$$

Here ν_a^{FIS} is the change of the frequency of an atomic transition (numerated by index a) which is caused by the change of nuclear size and shape between two isotopes; $\delta \langle r^2 \rangle$ is the change of the nuclear rms radii squared, $\delta \langle r^2 \rangle = \langle r^2 \rangle_2 - \langle r^2 \rangle_1$ and $\delta \langle r^4 \rangle = \langle r^4 \rangle_2 - \langle r^4 \rangle_1$.

First term in Eq. (3) is the standard FIS; the other two terms are corrections responsible for the nonlinearity of the King plot. The term with $G_a^{(2)}$ is due to the second-order effect in the change of the nuclear Coulomb potential called the quadratic field shift (QFS) and the last term appears mainly due to the relativistic effects in the electron wave function; i.e., these terms represent different physical phenomena. On the other hand, their effects on the isotope shift are similar. It was suggested in Ref. [1] that $\langle r^4 \rangle$ and $\langle r^2 \rangle$ are related by $\langle r^4 \rangle = b \langle r^2 \rangle^2$, where b is just a numerical constant, $b = 1.32$. Extra care should be taken in calculating $G^{(2)}$ and $G^{(4)}$ independently on each other. For example, they cannot be defined

simultaneously in a fitting procedure. Therefore, we start the calculations by eliminating the QFS term, i.e., by considering FIS in the linear approximation. The change of the nuclear Coulomb potential between two isotopes is considered as a perturbation and is treated in the first order using the random phase approximation (RPA). The RPA equations for core electrons have the following form [7]:

$$(\hat{H}^{\text{HF}} - \epsilon_c)\delta\psi_c = -(\delta V_N + \delta V_{\text{core}})\psi_c, \quad (4)$$

where δV_N is the difference between nuclear potentials for the two isotopes, index c numerates states in the core, and δV_{core} is the change of the self-consistent HF potential induced by δV_N and the changes to all core functions $\delta\psi_c$. Equations (4) are solved self-consistently for all states in the core with the aim of finding δV_{core} . The FIS for a valence state v is then given by

$$v^{\text{FIS}} = \langle \psi_v^{\text{BO}} | \delta V_N + \delta V_{\text{core}} | \psi_v^{\text{BO}} \rangle. \quad (5)$$

Apart from eliminating the QFS, an important advantage of using the RPA method (where the small parameter, i.e., the change of the nuclear radius, is explicitly separated) is the suppression of a numerical noise. Nonlinearity of the King plot is extremely small and direct full scale calculations of the change of the atomic electron energy due to a tiny change of the nuclear radius (i.e., without the separation of the small parameter) may lead to a false effect in the King plot nonlinearity (see below). After FIS is calculated for a range of nuclear parameters, the constants F_a and $G_a^{(4)}$ are found by fitting the results of the atomic calculations by formula (3) (without $G^{(2)}$) by the least-square-root method.

To calculate $G^{(2)}$, we use the second-order perturbation theory

$$G_a^{(2)} = \sum_n \frac{\langle a | \delta V_N + \delta V_{\text{core}} | n \rangle^2}{E_a - E_n} / \delta \langle r^2 \rangle^2. \quad (6)$$

Here δV_N is the change of nuclear potential between two isotopes. Summation goes over complete set of the single-electron basis states, including states in the core and negative-energy states. To include the core-valence correlations, one can use BO for single-electron states a and n . Again, the perturbation theory is used instead of the direct calculation of the change of the electron energy due to the tiny change of the nuclear radius to suppress numerical noise.

Instead of the direct summation over electron states in Eq. (6), one can first solve the RPA equation for the valence state a

$$(\hat{H}^{\text{HF}} + \hat{\Sigma} - \epsilon_a)\delta\psi_a^{\text{BO}} = -(\delta V_N + \delta V_{\text{core}})\psi_a^{\text{BO}}, \quad (7)$$

and then use

$$G_a^{(2)} = \langle \delta\psi_a^{\text{BO}} | \delta V_N + \delta V_{\text{core}} | \psi_a^{\text{BO}} \rangle / \delta \langle r^2 \rangle^2. \quad (8)$$

We obtain the same results using Eqs. (6) and (8). This provides a test of the numerical accuracy.

Nuclear deformation. The quadrupole nuclear deformation β provides a measure of the deviation of the nuclear density distribution from spherical shape so that nuclear radius $r_n(\theta)$ in the θ direction with respect of the axis of symmetry is written as $r_n(\theta) = r_0(1 + \beta Y_{20}(\theta))$. Electron feels nuclear density averaged over the nuclear rotation (see, e.g., Ref. [6]).

TABLE I. Calculated parameters of formula (3) for the FIS in two transitions of Yb^+ ; a stands for the $6s_{1/2}-5d_{5/2}$ transition and b stands for the $6s_{1/2}-5d_{3/2}$ transition. Case 1 corresponds to deformed nuclei, while case 2 corresponds to spherical nuclei.

Case	Transition	F (GHz/fm ²)	$G^{(2)}$ (GHz/fm ⁴)	$G^{(4)}$ (GHz/fm ⁴)
1	a	-17.6035	0.02853	0.01308
	b	-18.0028	0.02853	0.01337
2	a	-18.3026	0.02853	0.01245
	b	-18.7201	0.02853	0.01273

We calculate the average density by integrating the deformed density over θ .

To determine the values of F and $G^{(4)}$ parameters in Eq. (3), we first vary the nuclear root-mean-square (rms) charge radius r_c and the quadrupole deformation parameter β in the range determined by the nuclear theory (see below): $5.234 \text{ fm} \leq r_c \leq 5.344 \text{ fm}$ and $0.305 \leq \beta \leq 0.345$, and then fit the F and $G^{(4)}$ parameters by the formula (see also Refs. [6,11])

$$v^{\text{FIS}} = F\delta\langle r^2 \rangle + G^{(4)}\delta\langle r^4 \rangle \quad (9)$$

to the results of atomic calculations of FIS for different r_c and β . The values of F and $G^{(4)}$ parameters defined in such a way are presented in Table I. The table also gives the values of the $G^{(2)}$ parameters calculated using (6) and (8). Note that FIS for the d states of Yb^+ is about two orders of magnitude smaller than FIS for the $6s$ states and in QFS small matrix elements for the d states appear in the second order while in the calculations of F are in the first order. Therefore, the relative difference in the $G^{(2)}$ parameters for the $s-d_{3/2}$ and $s-d_{5/2}$ transitions is much smaller than the relative difference for the F parameters. Note that nonlinearities of the King plot are sensitive to the tiny differences in the ratios F_a/F_b , $G_a^{(2)}/G_b^{(2)}$, and $G_a^{(4)}/G_b^{(4)}$ [see Eq. (11) and discussion below it]. Therefore, we keep four digits for $G^{(2)}$ and $G^{(4)}$ to avoid the effect of rounding on the nonlinearity.

It was shown in Ref. [1] that $\langle r^4 \rangle \approx b\langle r^2 \rangle^2$, where b is just a numerical constant, $b = 1.32$ [1]. We found that the situation is different in deformed and spherical nuclei. By calculating $\langle r^4 \rangle$ in both cases, we found that the results can be fitted with high accuracy by the formula

$$\langle r^4 \rangle = [b_0 + b_1(r_c^2 - r_0^2) + b_2(\beta - \beta_0)]r_c^2, \quad (10)$$

where $r_0 = 5.179 \text{ fm}$ and $\beta_0 = 0.305$. For deformed nuclei $b_0 = 1.3129$, $b_1 = -0.0036$, $b_2 = 0.1$, while for spherical nuclei $b_0 = 1.2940$, $b_1 = -0.0038$, $b_2 = 0$.

To study the nonlinearity of the King plot, we need total isotope shift (including mass shift) for two transitions a and b . Then, using Eq. (3), one can write for the isotope shift between isotopes i and j

$$\begin{aligned} \frac{v_{bij}}{\mu_{ij}} = & \frac{F_b}{F_a} \frac{v_{aij}}{\mu_{ij}} + \left(K_b - \frac{F_b}{F_a} K_a \right) + \left(G_b^{(2)} - \frac{F_b}{F_a} G_a^{(2)} \right) \frac{\delta \langle r^2 \rangle_{ij}^2}{\mu_{ij}} \\ & + \left(G_b^{(4)} - \frac{F_b}{F_a} G_a^{(4)} \right) \frac{\delta \langle r^4 \rangle_{ij}}{\mu_{ij}}. \end{aligned} \quad (11)$$

TABLE II. The deviations from the linearity of the King plot (in parts of 10^{-6}). The comparison between experiment [1] and calculations in different nuclear models.

Isotope pair	Expt.	Nuclear model					
		BETA	FIT	NL3*	DD-ME2	DD-ME δ	DDPC1
168,170	-0.192	0.642	-0.206	-0.037	-0.084	-0.511	-0.080
170,172	0.270	-0.607	0.281	-0.159	-0.467	0.546	-0.222
172,174	-0.489	-3.05	-0.523	-0.200	-0.028	0.392	-0.198
174,176	0.411	3.03	0.448	0.387	0.551	-0.406	0.472

Here v_{bij} is the total isotope shift for the transition b which is related to FIS [see formula (3)] by $v_{bij} = v_{bij}^{\text{FIS}} + K_b \mu_{ij}$, K is the electron structure factor for the mass shift, and $\mu = 1/m_i - 1/m_j$ is the inverse mass difference. The meaning of all other parameters in (11) is the same as in (3). The first line of Eq. (11) corresponds to the standard King plot, and the second and third lines contain the terms which may cause the King plot nonlinearities. To calculate isotope shift and build King plot using (11), we use the calculated parameters F , $G^{(2)}$, $G^{(4)}$ from Table I, the values of K and μ from Ref. [1], and the values of the change of nuclear parameters $\delta\langle r^2 \rangle_{ij}$ and $\delta\langle r^4 \rangle_{ij}$ which come from several nuclear models (see below).

To study these nonlinearities, we use the least-square fitting of Eq. (11) by the formula $v'_b = Av'_a + B$, where $v' = v/\mu$. The relative nonlinearities are calculated as $\Delta v'_b/v'_b$, where $\Delta v'_b$ is the deviation of the isotope shift v'_b from its linear fit. To do the fitting and making King plot, we need to know the change of nuclear parameters $\delta\langle r^2 \rangle$ and $\Delta\beta$ between the isotopes of interest. We use nuclear calculations for this purpose using a range of nuclear models. They include the empirical model named BETA, the parameters of which are determined from experimental data, the hypothetical model (labeled as FIT), the parameters of which are defined by the fit of nuclear parameters to experimental FIS and the deviations of King plot from nonlinearity, and the fully self-consistent covariant density functional theory (CDFT) with several functionals such as DD-ME2, DD-ME δ , NL3*, and DD-PC1 [12,13]. Nuclear parameters of the Yb isotopes with even neutron number obtained in these models are presented in the Supplemental Material [14].

Using the parameters coming from these models, we calculate FIS, build the King plot, find its deviations from the linearity, and compare the results to the experimental data from Ref. [1]. The results are presented in Table II and Fig. 1. One can see that the values of the experimental and theoretical nonlinearities are of the same order of magnitude for all nuclear models. The FIT model presents almost perfect fit of the experimental data for both isotope shift and the nonlinearities. For some models (e.g., BETA, FIT, NL3*, DDPC1¹) there is a strong correlation between experimental and theoretical data. This means that the nuclear deformation is an important effect which has to be included into the analysis.

The origin of nonlinearity in the King plot in deformed nuclei could also be understood from nuclear theory perspective. The single-particle states are twofold degenerate in deformed

nuclei and the increase of neutron Fermi level with increasing neutron number leads to the change of the occupation of the pairs of different single-particle states, emerging from different spherical subshells, located in the vicinity of neutron Fermi level. These pairs contribute differently to the charge radii and deformations of the nucleus. As a consequence, both charge radii and deformations obtained in the CDFT calculations as a function of neutron number show some staggering with respect of averaged smooth trend (see the Supplemental Material [14]). The situation is different for the Ca^+ ions in the chain of $^{40-48}\text{Ca}$ isotopes [15] since they do not show significant nonlinearities in the King plot. This is because these nuclei are spherical and they are built by the occupation of mostly neutron $f_{7/2}$ subshell with increasing neutron number.

Quadratic field shift. Reference [1] argues that QFS is the main source of the nonlinearity of the King plot. However, their calculations only provided an upper limit on the nonlinearity since the results of CI (configuration interaction) and MBPT calculations were very different. From our point of view, the problem with the calculations in Ref. [1] is that they have not separated a small parameter, the change of the nuclear radius, and obtained FIS from the small difference in

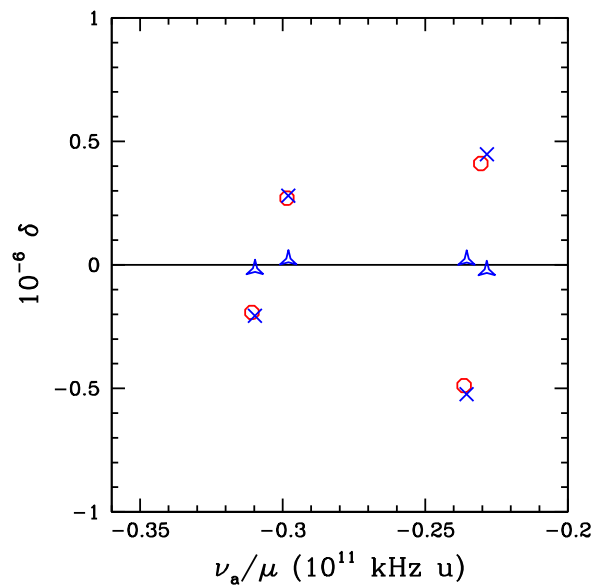


FIG. 1. The deviations from linear King plot in experiment (solid red circles) and theory. Theoretical deviations caused by nuclear deformation are shown as blue crosses, and those by QFS are shown as blue triangles. All theoretical numbers correspond to the FIT nuclear model.

¹We label the CDFT model by employed functional.

TABLE III. The deviations from the linearity of the King plot δ due to the quadratic field shift. The comparison between experiment [1] and calculations using the $\delta\langle r^2 \rangle$ values which fit the experimental isotope shift [1]. The deviation δ is shown as a function of v_a/μ [see Eq. (11)].

Isotope pair	Expt.		QFS	
	v_a/μ	δ	v_a/μ	δ
	10^{11} kHz u	10^{-6}	10^{11} kHz u	10^{-6}
168,170	-0.311	-0.192	-0.351	-0.017
170,172	-0.299	0.270	-0.337	0.020
172,174	-0.236	-0.489	-0.272	0.013
174,176	-0.231	0.411	-0.267	-0.016

the energies of the atomic transitions calculated for different nuclear radii. This is certainly a good approach for the calculation of FIS but it is not good enough to calculate a very small nonlinearity which is extremely sensitive to numerical noise.

Our results presented earlier indicated that QFS gives a much smaller contribution to the nonlinearity of the King plot than the upper limit presented in Ref. [1]. To test this result, we performed FIS and QFS calculations by a different method assuming that all isotopes have spherical nuclear shape ($\beta = 0$). The main motivation for using RPA method in the case of nuclear deformation is the minimization of numerical noise which comes from extra integration over directions. There is no such problem for spherical nuclei and the procedure is less complicated. FIS in this case may be found from the direct variation of the nuclear radius in the nuclear Coulomb potential. We perform HF and BO calculations for a range of nuclear charge rms radii from $\langle r^2 \rangle = (5 \text{ fm})^2$ to $\langle r^2 \rangle = (6 \text{ fm})^2$ and present the results by the same formula (3) (see Table I). As in case of deformed nuclei, the QFS parameter $G^{(2)}$ is found from the perturbation theory calculations. The values of F and $G^{(4)}$ are slightly different.

The same equation (11) and the same procedure were used to find the nonlinearities of the King plot. The results are presented on Fig. 1 and Table III. As one can see, the nonlinearity caused by QFS is an order of magnitude smaller than the observations. It is also much smaller than the nonlinearity caused by the variation of the nuclear deformation.

We also performed another test calculation using constant value $\beta = 0.3$ instead of $\beta = 0$. Again, without variation of β the nonlinearity of the King plot is small.

The change of nuclear rms charge radius. Formula (3) with parameters F , $G^{(2)}$, $G^{(4)}$ from Table I can be used to find the change of the nuclear rms charge radius between isotopes by fitting experimental FIS. The values of the $\delta\langle r^2 \rangle$ corresponding to the best fit (the FIT model) are presented in Table IV as case A and compared with other data.

It is widely assumed in the atomic community that FIS is described by a variation of a single parameter $\langle r^2 \rangle$, i.e., the change of higher nuclear momenta are ignored. On the other hand, it is claimed in Ref. [1] that inclusion of the variation of $\langle r^4 \rangle$ (which is also proportional to $\delta\langle r^2 \rangle$) can change $\delta\langle r^2 \rangle$ extracted from the FIS experimental data by about 7%. The term with $\delta\langle r^4 \rangle$ is also included in our analysis above. It is important to check what happens if this term is excluded. To

TABLE IV. The changes of nuclear rms charge radius ($\delta\langle r^2 \rangle$, fm²) extracted from the isotope shift measurements. Case A of the present work corresponds to formula (3) while case B corresponds to formula (12).

Isotope pairs	Ref. [1]		Ref. [16,17]	This work	
	CI	MBPT		A	B
	(168,170)	0.156		0.149	0.1561(3)
(170,172)	0.146	0.140	0.1479(1)	0.130	0.129
(172,174)	0.115	0.110	0.1207(1)	0.102	0.101
(174,176)	0.110	0.105	0.1159(1)	0.097	0.096

do this, we perform different fitting of the RPA results. Instead of using (9), we use the expression in which the change of nucleus is reduced to the variation of $\langle r^2 \rangle$,

$$v^{\text{FIS}} = F\delta\langle r^2 \rangle + G_{\text{total}}^{(2)}\delta\langle r^2 \rangle^2. \quad (12)$$

To fit the experimental data, we add to $G_{\text{RPA}}^{(2)}$ the second-order $G^{(2)}$ from Table I, $G_{\text{total}}^{(2)} = G^{(2)} + G_{\text{RPA}}^{(2)}$. The resulting F , $G_{\text{RPA}}^{(2)}$, $G_{\text{total}}^{(2)}$ coefficients for two transitions in Yb⁺ are presented in Table V. Then we use these numbers to fit the experimental FIS by adjusting the values of $\delta\langle r^2 \rangle$. The resulting values of $\delta\langle r^2 \rangle$ are presented in Table IV as case B. They are practically the same as in case A. We conclude that neglecting $G^{(4)}$ actually leads to the redefinition of the parameter F but practically does not affect value of $\delta\langle r^2 \rangle$ extracted from the experiment.

The comparison with other results for $\delta\langle r^2 \rangle$. It is instructive to analyze possible reasons for the difference between our results and other results for $\delta\langle r^2 \rangle$ presented in Table IV. There is a 12–19% difference between our results and those published in Ref. [16] (see Table IV). However, the latter were taken from a 50-year-old paper [17], which has no many-body calculations but only estimations based on the single-electron consideration. The uncertainty of such estimations can be well above 10% and even 20%.

There is also a 8–13% difference between our results and those of Ref. [1]. Reference [1] contains two calculations of the FIS constants performed by CI and MBPT methods with 4% difference between corresponding results. Our FIS constant F is about 13% larger than the same constant calculated in Ref. [1] using the CI method and about 8% larger than those calculated in Ref. [1] using the MBPT method. This explains the difference in the results for $\delta\langle r^2 \rangle$ (Table IV). When we use the numbers from Ref. [1] in Eq. (3), we reproduce their results for $\delta\langle r^2 \rangle$. The difference in the results

TABLE V. Calculated parameters of formula (12) for the FIS in two transitions of Yb⁺.

Transition	F (GHz/fm ²)	$G_{\text{RPA}}^{(2)}$ (GHz/fm ⁴)	$G_{\text{total}}^{(2)}$ (GHz/fm ⁴)
<i>a</i>	-16.7185	0.015534	0.044064
<i>b</i>	-17.0984	0.015883	0.044413

seems to be due to the difference in the procedures defining the constants F and G . We use BO and the RPA method to calculate F and $G^{(4)}$ and the perturbation theory to find $G^{(2)}$, as explained above. The authors of Ref. [1] calculate F as a leading term of the Seltzer moment expansion at the origin for the total electron density (see Eq. (S11) in Ref. [1]) and then use partial derivatives of FIS to calculate constants G . Such method looks sensitive to the degeneracy of $G^{(2)}$ and $G^{(4)}$ contributions to FIS. An indication of the problem may be a significant relative difference in $G^{(2)}$ parameters in Ref. [1], while we argued above that it must be very small since it appears in the second order of the small d -wave FIS matrix elements.

It is instructive to explain why the ratios $G^{(4)}/F$ are different in the s - $d_{3/2}$ and s - $d_{5/2}$ transitions (this is needed for the nonlinearity of the King plot without QFS). We suggest the following mechanism supported by the numerical calculations. According to it, only two relativistic Dirac wave functions, $s_{1/2}$ and $p_{1/2}$, penetrate into the nucleus. They have different spatial distributions inside and therefore the ratios of the $\delta\langle r^2 \rangle$ and $\delta\langle r^4 \rangle$ contributions to their energies and wave

functions are noticeably different. The $d_{3/2}$ and $d_{5/2}$ wave functions interact differently with the $s_{1/2}$ and $p_{1/2}$ ones and this gives the difference in $G^{(4)}/F$.

In conclusion, we state that presented arguments indicate that nuclear deformation is the most likely source of recently observed nonlinearities of King plot in Yb^+ . The results of the combined nuclear and atomic calculations for the effect are consistent with the observations. The contribution of the QFS is about an order of magnitude smaller. The measurements of the nonlinearity of the King may be used to study nuclear deformation in nuclei with zero spin where nuclear electric quadrupole moment cannot be extracted from atomic spectroscopy. The changes of nuclear charge RMS radii between even-even Yb isotopes extracted from atomic measurements are consistent with nuclear theory.

Acknowledgments. We are grateful for J. Berengut for useful discussion. The work was supported by the Australian Research Council Grants No. DP190100974 and No. DP200100150 and by the US Department of Energy, Office of Science, Office of Nuclear Physics under Grant No. DE-SC0013037.

-
- [1] I. Counts, J. Hur, D. P. L. Aude Craik, H. Jeon, C. Leung, J. C. Berengut, A. Geddes, A. Kawasaki, W. Jhe, and V. Vuletic, *Phys. Rev. Lett.* **125**, 123002 (2020).
- [2] K. Mikami, M. Tanaka, and Y. Yamamoto, *Eur. Phys. J. C* **77**, 896 (2017).
- [3] Evaluated Nuclear Structure Data File (ENSDF) located at the website (<http://www.nndc.bnl.gov/ensdf/>) of Brookhaven National Laboratory. ENSDF is based on the publications presented in Nuclear Data Sheets (NDS), which is a standard for evaluated nuclear data.
- [4] S. G. Nilsson and I. Ragnarsson, *Shapes and Shells in Nuclear Structure* (Cambridge University Press, Cambridge, UK, 1995).
- [5] Z.-H. Zhang, M. Huang, and A. V. Afanasjev, *Phys. Rev. C* **101**, 054303 (2020).
- [6] S. O. Allehabi, V. A. Dzuba, V. V. Flambaum, A. V. Afanasjev, and S. E. Agbemava, *Phys. Rev. C* **102**, 024326 (2020).
- [7] V. A. Dzuba, V. V. Flambaum, P. G. Silvestrov, and O. P. Sushkov, *J. Phys. B: At. Mol. Phys.* **20**, 1399 (1987).
- [8] V. A. Dzuba and V. V. Flambaum, *Phys. Rev. A* **77**, 012515 (2008).
- [9] V. A. Dzuba and V. V. Flambaum, *Phys. Rev. A* **83**, 052513 (2011).
- [10] V. A. Dzuba, V. V. Flambaum, M. S. Safronova, S. G. Porsev, T. Pruttivarasin, M. A. Hohensee, and H. Häffner, *Nat. Phys.* **12**, 465 (2016).
- [11] V. V. Flambaum and V. A. Dzuba, *Phys. Rev. A* **100**, 032511 (2019).
- [12] A. V. Afanasjev and S. E. Agbemava, *Phys. Rev. C* **93**, 054310 (2016).
- [13] S. E. Agbemava, A. V. Afanasjev, D. Ray, and P. Ring, *Phys. Rev. C* **89**, 054320 (2014).
- [14] Please see Supplemental Material at <http://link.aps.org/supplemental/10.1103/PhysRevA.103.L030801> for more information on nuclear models used in the calculations.
- [15] C. Solaro, S. Meyer, K. Fisher, J. C. Berengut, E. Fuchs, and M. Drewsen, *Phys. Rev. Lett.* **125**, 123003 (2020).
- [16] I. Angeli and K. P. Marinova, *At. Data Nucl. Data Tables* **99**, 69 (2013).
- [17] D. L. Clark, M. E. Cage, D. A. Lewis, and G. W. Greenlees, *Phys. Rev. A* **20**, 239 (1979).